Progress In Electromagnetics Research C, Vol. 136, 189–198, 2023

Dual Band MIMO Antenna with High Isolation for GSM and WLAN Applications

Alka Khade, Mahadu A. Trimukhe, Shubhangi M. Verulkar, and Rajiv K. Gupta*

Abstract—We propose a compact dual-band MIMO antenna for GSM 1800 MHz and WLAN applications. A novel single branch dual band antenna consisting of a quarter annular ring and an inverted U-shaped strip is designed by decreasing the electromagnetic coupling between higher order modes of an annular ring ultra-wideband (UWB) antenna, and a simple technique of slots and I and L-shaped stubs protruding from ground plane is employed to achieve high isolation. $S_{11} < -10$ dB over 1.704–1.934 GHz and 5.66–6.25 GHz frequency range and mutual coupling $S_{12} < -20$ dB and < -28 dB over the two bands are achieved. The radiation pattern, envelope correlation coefficient (ECC), total active reflection coefficient (TARC), diversity gain (DG), and mean effective gain (MEG) conform to MIMO specifications. The prototype antenna is fabricated on a $0.244\lambda_0 \times 0.17\lambda_0$ FR4 substrate, where λ_0 is the free-space wavelength at 1.7 GHz. The antenna offers stable radiation patterns. The antenna is compact, simple to design, easy to fabricate, and low in cost. These characteristics depict the suitability of this antenna for portable wireless devices.

1. INTRODUCTION

Multiple-Input Multiple-Output (MIMO) antenna fulfils the desired requirements of high data rate, huge capacity, and high throughput of wireless communication system as it is less susceptible to multipath fading [1]. However, mutual coupling between multiple elements, positioned closely in a compact volume, degrades the system performance which causes the biggest hurdle in improving the data rate of wireless system [2]. Therefore, different isolation techniques such as split ring resonator (SRR) structures, electromagnetic bandgap (EBG) structures, neutralization line, and defected ground structures (DGS) are incorporated in [3, 4]. An array of EBG and fractal EBG unit cell are designed to enhance the isolation between two microstrip antenna elements [5–7]. Human face shaped ultra-wideband (UWB) MIMO antenna is designed. Slots are etched, and elliptical shape is modified to enhance the bandwidth, and rectangular and triangular slots are etched in ground plane to enhance the isolation [8]. Annular slot DGS [9] and rectangular slot and inverted L shaped stub [10] are used to improve the isolation. Elliptical slot and parasitic strip are incorporated between two closely spaced F shaped monopole antennas [11]. Defected ground and stubs are used between two orthogonally placed pie-shaped slotted rectangular patches [12]. T-shaped strip in the ground plane is embedded in [13]. Vertical strips, quasi-pai shaped slots, and a neutralization line are deployed to improve the isolation in [14]. DGS, T-shaped parasitic element, and branches extending from ground plane are used to increase the isolation in [15]. An elliptical curve-shaped branch extending from ground plane is used as a decoupling structure to improve the isolation over wideband [16]. Orthogonally placed two trapezoidal radiating elements with a rectangular stub in the ground offer high isolation [17]. A UWB MIMO antenna with orthogonally placed quad elements is designed on a flexible substrate for 5G and wearable applications [18]. Ring shaped slots in the ground are incorporated to obtain desired isolation between two crescent-shaped

Received 1 June 2023, Accepted 4 August 2023, Scheduled 20 August 2023
* Corresponding author: Rajiv Kumar Gupta (rajivgupta@ternaengg.ac.in).
The authors are with the Department of Electronics and Telecommunication, Terna Engineering College, Navi-Mumbai, India.

antenna elements [19]. High isolation is achieved by placing spiral resonating unit cells between two antenna elements [20]. Stepped L-shaped slots are used in a dual-band MIMO antenna [21]. The isolation is improved by using a meander line decoupling structure protruding from the ground plane between two monopole antennas [22]. Orthogonal polarization diversity is used to achieve good isolation among multiple antenna elements [23–25]. Four antenna elements with parasitic patches are orthogonally placed to achieve the desired isolation [26, 27].

In this work, a compact dual-band MIMO antenna for GSM 1800, and WLAN applications is proposed. The MIMO antenna system consists of two mirror-image monopole radiating elements each consisting of a quarter annual ring and an inverted U-shaped strip. Slots and stubs in the ground are incorporated to achieve high isolation. $S_{12} < -20$ dB and -28 dB are obtained over 1.704–1.934 GHz and 5.66–6.25 GHz frequency range, respectively. Antenna offers a stable radiation pattern with ECC < 0.02 over the lower band and < 0.002 over the higher band. The antenna has smaller dimensions than the reported state of art antennas.

The rest of the paper is organized as follows. Section 2 of the paper deals with antenna geometry, evolution steps, and design theory. Isolation improvement using slots and stubs is also explained using surface current distribution in this section. Measurement results and performance parameters of the MIMO antenna are discussed in Section 3. The proposed antenna is compared with the antennas reported in the literature in Section 4. The conclusion is provided in Section 5.

2. ANTENNA GEOMETRY, EVOLUTION STEPS AND DESIGN THEORY

A monopole antenna excites a number of higher order modes each with wide bandwidth which couple electromagnetically to provide ultrawide bandwidth. However, a wideband antenna is not always desirable as it interferes with other narrow band wireless systems operating within the ultrawide bandwidth. Band notch UWB antennas or multiband antennas are designed to mitigate this problem. Traditionally, multiband antennas are designed using multiple branches in which each branch resonates over a band, and the length and width of a branch determine the resonant frequency and bandwidth of a band.

A novel single branch multiband antenna can be designed by decreasing the electromagnetic coupling between higher order modes by decreasing the thickness and selectively cutting the symmetrical portion of UWB antenna. Based on this concept a compact multiband antenna is designed [28]. The isolation between two elements of a multiband MIMO antenna is improved by using a simple technique of multiple ground slots and stubs. The rectangular stub acts as an inductor, and the spacing between the stubs acts as a capacitor, thus multiple stubs and the spacing between them act as band-stop filters which suppress surface-waves and improve the isolation over multiband. Stubs protruding from ground

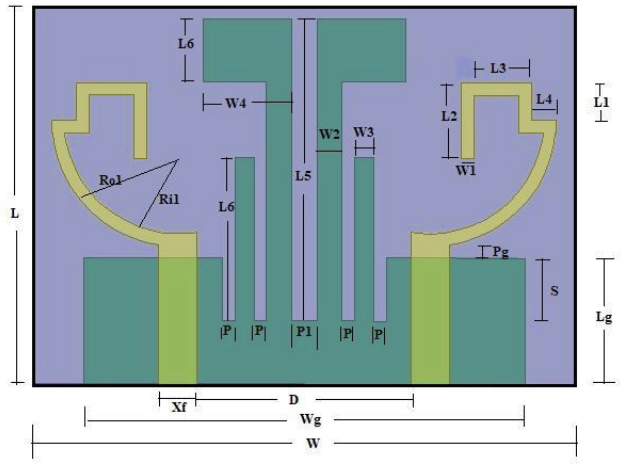

Figure 1. Geometry of the antenna.

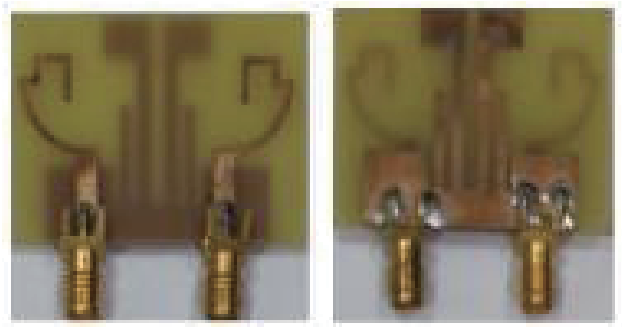

Figure 2. Fabricated prototype antenna. (a) Top view. (b) Bottom view.

plane also act as reflector to near fields and provide decoupling path to surface waves and thus, improve isolation.

The geometry of the antenna designed on a $0.17\lambda_0 \times 0.24\lambda_0$ ($30 \times 43\,\text{mm}^2$) substrate is shown in Fig. 1. Fig. 2 depicts the fabricated antenna. A 1.6 mm thick FR4 substrate ($\varepsilon_r = 4.4$ and $\tan\delta = 0.02$) is used to design the antenna which consists of two mirror-image monopoles placed $0.096\lambda_0$ (17 mm) apart. The antenna parameters are optimized and tabulated in Table 1.

Table 1. Optimized dimensional parameters of the antenna.

Parameters	L	W	Lg	Wg	Xf	D	Pg	$Ro1$	$Ri1$	$L1$	$L2$	$L3$
dimensions (mm)	30	43	10	33	3	17	1	10	9	3	6	4.5
Parameters	$L4$	$L5$	$L6$	$W1$	$W2$	$W3$	$W4$	S	P	$P1$		
dimensions (mm)	2	24	13	1	1	1.5	7	5	1	2		

Figure 3 depicts the different evolution stages of antenna. 'Ant 1' is designed by reducing the electromagnetic coupling between the higher-order modes of a UWB circular annular ring monopole antenna. The decrease in electromagnetic coupling between the higher-order modes results in miniaturization and multiband antenna. The electromagnetic coupling between higher order modes can be decreased by decreasing the thickness of UWB antenna and selectively cutting the symmetrical portion of UWB annular ring monopole antenna [28]. The monopole antenna 'Ant 1' is designed using a thin quarter annular ring, and then an inverted U-shaped strip is added to it to decrease the resonating frequency by increasing the effective path length. This antenna fabricated on a $26 \times 22\,\text{mm}^2$ substrate offers tri-band operation. $S_{11} < -10\,\text{dB}$ is obtained over 2.31–2.71 GHz, 5.21–5.88 GHz, and 8.9–9.5 GHz.

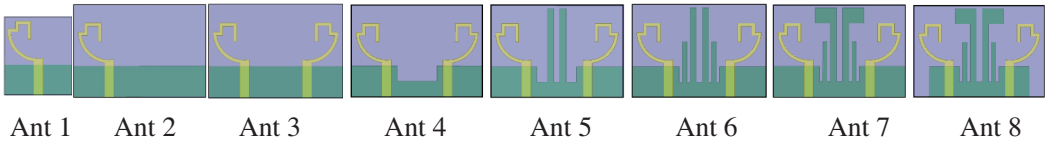

Figure 3. Evolution stages of antenna.

The ground plane is extended to accommodate the second element in 'Ant 2'. Ground plane dimensions affect the resonant frequency and the impedance matching of an antenna. Impedance matching degrades in 'Ant 2'. In 'Ant 3', the second element is added at edge-to-edge inter-element spacing of 17 mm or $0.1\lambda_0$, with λ_0 being the free-space wavelength at 1.7 GHz, lower frequency of the desired lower operating band (1.710–1.880 GHz). $S_{11} < -10\,\text{dB}$ is obtained over 2.5–2.75 GHz and 5.32–5.97 GHz in 'Ant 3'. However, the impedance matching as well as isolation is not satisfactory. The isolation at upper band is about 18 dB. To improve the isolation, a slot is cut in the ground plane in 'Ant 4'. The slot acts as a band-stop filter to surface waves, and it also increases the path length of the surface waves and thus improves the isolation. The isolation between the elements has increased in the upper band while there is negligible improvement in the lower band. In 'Ant 5', two long stubs protruding from the ground plane are added. These stubs provide a decoupling path to the surface waves and reflect the near fields. The resonant frequencies decrease due to the addition of stubs. The mutual coupling $< -11\,\text{dB}$ and $< -38\,\text{dB}$ are obtained in two bands, respectively. In 'Ant 6' two more stubs are added. It improves the isolation in the lower band but degrades the isolation in the upper band. The mutual coupling $< -13\,\text{dB}$ and $< -32\,\text{dB}$ are obtained over two bands, respectively. Since the surface current flows in the horizontal direction in radiator, $5 \times 5\,\text{mm}^2$ stubs are added to the long stubs to improve the mutual coupling in 'Ant 7'. The antenna operates over 1.71–1.97 GHz and 5.43–5.96 GHz. The mutual coupling $< -18\,\text{dB}$ and $< -32\,\text{dB}$ are obtained in two bands, respectively. The ground plane dimensions affect impedance matching as well as mutual coupling. The dimensions of

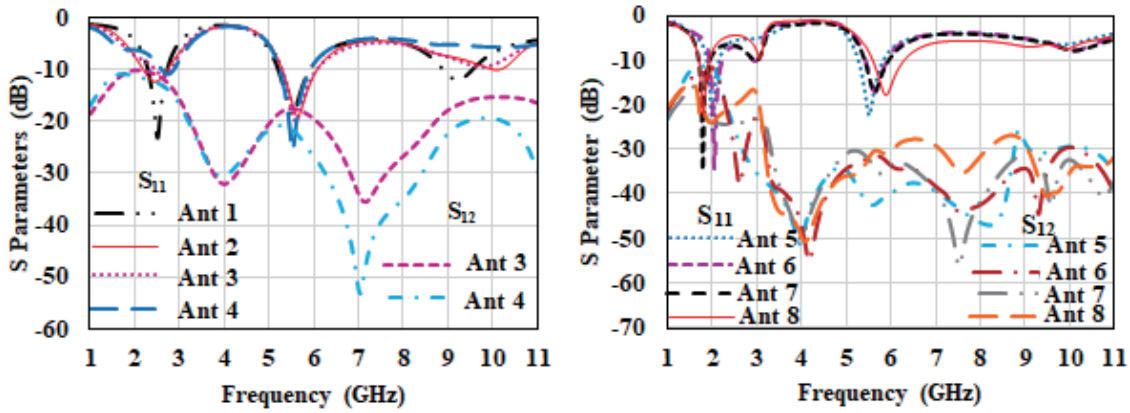

Figure 4. S parameters of evolution stages.

ground plane are decreased and optimized. The antenna operates over 1.704–1.934 GHz and 5.66–6.25 with $S_{12} < -20$ dB in the lower band and < -28 dB in the higher band. S-parameters of different stages of antenna are shown in Fig. 4.

The isolation is improved by using ground slots and stubs as shown in Fig. 4. The rectangular stubs act as inductors, and the spacing between the stubs acts as capacitor, thus the stubs and the spacing between them act as a band-stop filter which suppresses surface-waves. The slot in the ground plane increases the surface-waves path length and thus decreases mutual coupling. Two rectangular stubs and two inverted L shaped stubs, protruding from ground, also act as reflectors to near fields and form decoupling path. Thus, $S_{11} < -10$ dB and $S_{12} < -20$ dB over 1.704–1.934 GHz and $S_{12} < -28$ dB over 5.66–6.25 GHz are obtained as shown in Fig. 4.

The improvement in mutual coupling is also analyzed using surface current distribution. The scalar and vector surface current distributions of 'Ant 6' and 'Ant 8' are shown in Fig. 5 and Fig. 6, respectively. At lower band, the surface current is concentrated more in the inverted L stubs which offers effective decoupling paths, and as a result, mutual coupling < -20 dB is obtained. At higher band, the surface current is mainly concentrated in rectangular stub, and it acts as a decoupling path. Vector surface current distribution also confirms that the inverted L shaped stubs and rectangular stubs provide decoupling path at lower and higher bands, respectively. At lower band, the antenna operates in the fundamental mode, and higher-order modes are excited at higher band.

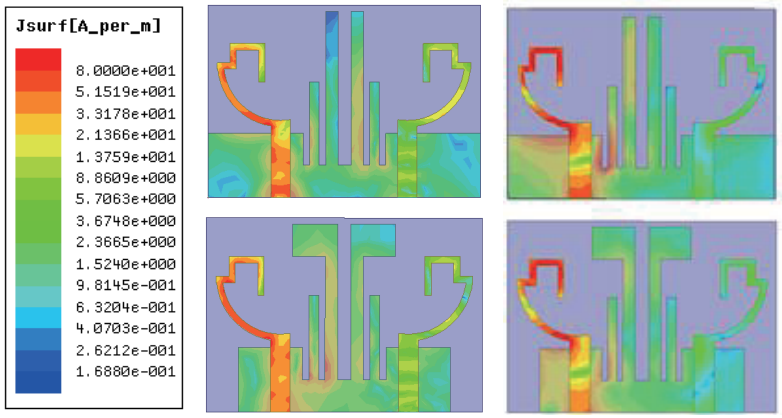

Figure 5. Scalar surface current distribution. (a) 1.8 GHz, (b) 5.9 GHz.

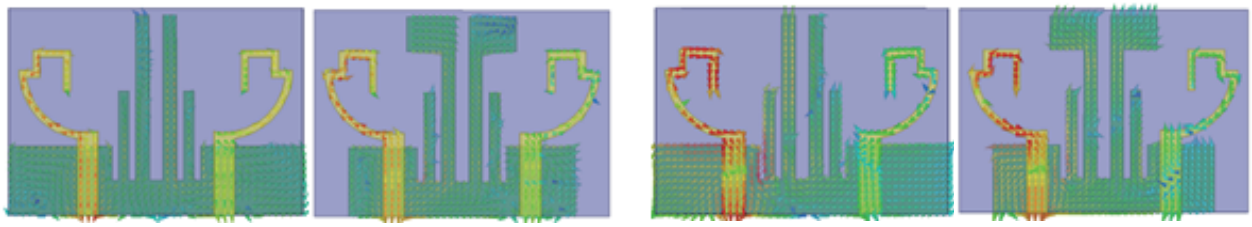

(a) (b)

Figure 6. Vector surface current distribution. (a) 1.8 GHz, (b) 5.9 GHz.

3. MEASURED RESULTS AND PERFORMANCE ANALYSIS

3.1. *S*-Parameters

S-parameters of prototype antenna (Fig. 2) are measured using Agilent-9916A network analyzer. S_{12} and S_{21} are measured by exciting one port while the other port is match-terminated. Measured *S*-parameters, shown in Fig. 7, agree with the simulated results. S_{11} and $S_{22} < -10$ dB is obtained over the desired bands. The mutual coupling S_{12} and $S_{21} < -20$ dB over the lower band and < -28 dB over the higher band are achieved.

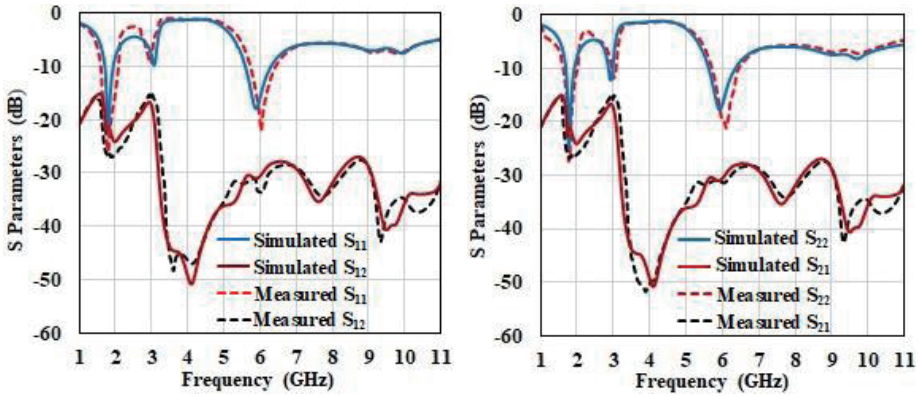

(a) (b)

Figure 7. *S*-Parameters of antenna.

3.2. Radiation Patterns and Diversity Performance

The radiation patterns of the MIMO antenna, obtained by exciting one port at a time and the other port match-terminated, are shown in Fig. 8. The radiation patterns at 'port 1' are almost mirror images of that at 'port 2' and therefore, confirm antenna diversity. The stable radiation patterns are nearly omnidirectional. The antenna offers peak gain of 1.4 dBi in the lower band, and gain increases to 4.1 dBi in the higher band. It provides maximum directivities of 2.8 dBi and 4.9 dBi and antenna efficiencies of 73% and 84% in lower and upper bands, respectively. The gain increases in higher band due to the increase in effective aperture area at higher frequencies.

The diversity performance of the MIMO antenna is analyzed by calculating diversity parameters such as ECC, DG, and MEG. ECC determines the isolation between communication channels. It considers the effect of radiating fields of one antenna on another when both antennas operate together. ECC based on the radiating fields, under uniform multipath indoor environment, is calculated [29]. ECC of antenna is less than 0.02 over 1.7–11 GHz as shown in Fig. 9.

The diversity gain is obtained from correlation coefficient using Equation (1) [29].

$$\mathrm{DG} = 10 \times \sqrt{(1 - |\mathrm{ECC}|)} \tag{1}$$

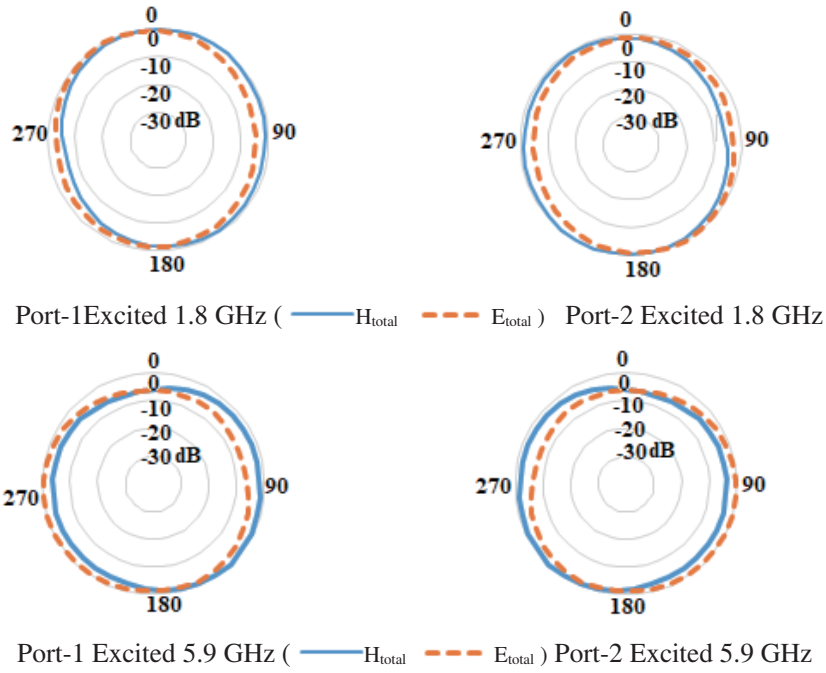

Figure 8. Radiation patterns of antenna.

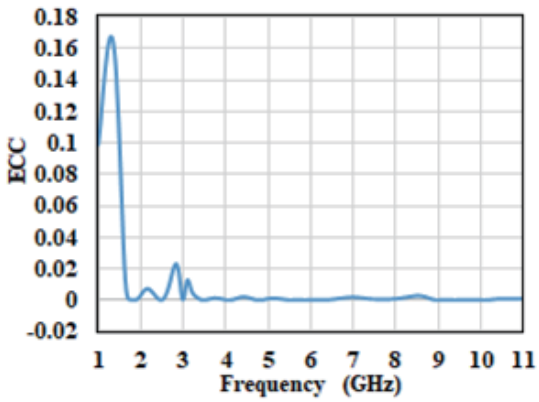

Figure 9. ECC of antenna.

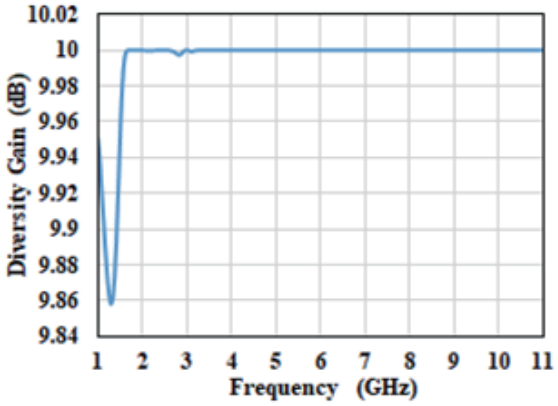

Figure 10. Diversity gain of antenna.

The calculated DG using Equation (1) [29] is around 10 dB throughout 1.7 GHz to 11 GHz frequency band indicating good diversity performance of antenna. DG plot is shown in Fig. 10.

Apart from ECC, the antenna must satisfy the following criteria with respect to Mean Effective Gain (MEG) as given in Equation (2).

$$\mathrm{MEG}_i/\mathrm{MEG}_j \cong 1 \tag{2}$$

where MEG_i and MEG_j are MEGs of the ith and jth antennas. MEG is derived using (3) [24].

$$\mathrm{MEG} = \int_0^{2\pi}\int_0^{\pi}\left[\frac{\mathrm{XPR}}{1+\mathrm{XPR}}\cdot P_\theta(\theta,\varphi)\cdot G_\theta(\theta,\varphi) + \frac{1}{1+\mathrm{XPR}}\cdot P_\varphi(\theta,\varphi)\cdot G_\varphi(\theta,\varphi)\right]\sin\theta d\theta d\varphi \tag{3}$$

where,

$$\mathrm{XPR} = \frac{\int_0^{2\pi}\int_0^{\pi} G_\theta(\theta,\varphi)\cdot\sin\theta d\theta d\varphi}{\int_0^{2\pi}\int_0^{\pi} G_\varphi(\theta,\varphi)\cdot\sin\theta d\theta d\varphi} \tag{4}$$

XPR expressed in Equation (4) is the cross-polarization ratio; $G_\theta(\theta\varphi)$ and $G_\varphi(\theta\varphi)$ are the gain of the antenna. $P_\theta(\theta\varphi)$ and $P_\varphi(\theta\varphi)$ are angular density functions of the incoming plane waves. MEG1, MEG2 and MEG1/MEG2 are calculated and shown in Fig. 11. MEG1 and MEG2 are quite identical, and the

Table 2. Comparison with reported antennas (*NR-Not reported).

Ref.	Technique employed for Isolation	Bands (GHz)	Minimum Isolation (dB)	Size $\lambda_0 \times \lambda_0 = \lambda_0^2$	ECC	DG (dB)
[9]	Annular slot in the ground plane	2.3–2.68 1.73–2.28	22 10	$0.29 \times 0.64 = 0.184$	< 0.012	DG-NR
[11]	Elliptical slot in ground plane and a rectangular parasitic strip	3.2–3.8 5.7–6.2	20 20	$0.32 \times 0.28 = 0.089$	< 0.03	DG > 9.8
[12]	Orthogonal polarisation diversity and slots and stubs in the ground plane	2.82–8.21 9.8–12.42	18 16	$0.24 \times 0.38 = 0.091$	< 0.0001	DG > 9.9
[13]	T-shaped metallic strip embedded in the defected ground plane	1.85–3.63 5.07–7.96	17.2 22.4	$0.28 \times 0.19 = 0.053$	< 0.003	DG ≈ 10
[14]	A neutralization line, slots and two stubs in the ground plane	2.12–2.66 5.09–5.42	15 15	$0.2 \times 0.27 = 0.054$	< 0.005	DG-NR
[15]	slots and stub in the ground plane, and parasitic element	3.41–3.60 4.76–5.04	29 41.4	$0.44 \times 0.66 = 0.29$	< 0.005	DG-NR
[17]	Orthogonal polarisation diversity and rectangular stub in ground plane	2.25–3.15 4.89–5.95	15 15	$0.375 \times 0.375 = 0.141$	< 0.003 < 0.01	DG > 9.99 DG > 9.95
[19]	Two interlaced ring-shaped slots in ground plane	2.1–2.9 5.13–5.85	19.3 55	$0.28 \times 0.33 = 0.093$	$< 0:017$ $< 0:004$	DG-NR
[20]	Complementary two-turn spiral resonator (CSRR)	2.34–2.47 3.35–3.67	32 18	$0.34 \times 0.21 = 0.071$	< 0.1	DG-NR
[21]	Open-ended slot in ground plane	2.6–3.1 5.42–6.2	21.2 23	$0.38 \times 0.28 = 0.1064$	< 0.08 < 0.1	DG > 9.59 DG > 9.48
[22]	Meandered line decoupling resonator	2.4–2.48 5.15–5.83	25 25	$0.48 \times 0.48 = 0.23$	< 0.08	DG-NR
This Work	Stubs and slots in the ground plane	1.7–1.93 5.66–6.25	20 28	$0.244 \times 0.17 = 0.0415$	< 0.02 < 0.002	DG > 9.99 DG > 9.99

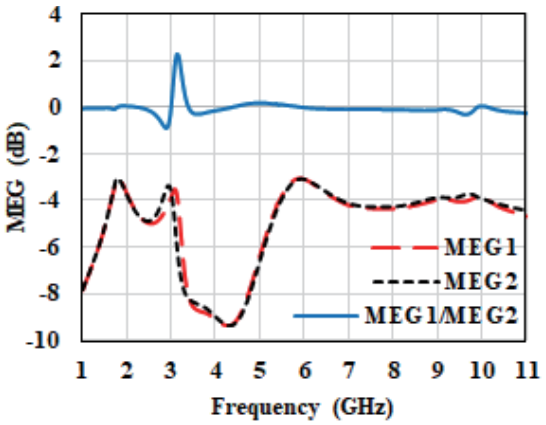

Figure 11. MEG of antenna.

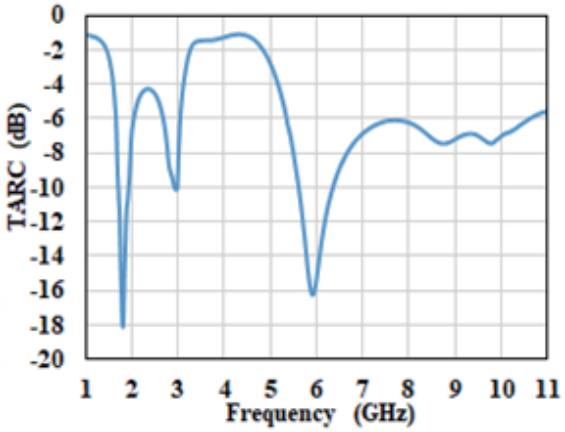

Figure 12. TARC of antenna.

ratio MEG1/MEG2 is close to 0 dB over the desired bands.

TARC (Γ) is calculated using Equation (5) [29] and shown in Fig. 12.

$$\text{TARC} = \frac{\sqrt{\left(\left|S_{11} + S_{12}e^{j\theta}\right|\right)^2 \left(\left|S_{21} + S_{22}e^{j\theta}\right|\right)^2}}{\sqrt{2}} \tag{5}$$

4. COMPARISON WITH REPORTED ANTENNAS

The designed MIMO antenna is compared with reported antennas in terms of the electrical-size, bandwidth, isolation, ECC, and DG in Table 2. The dual-band MIMO design is smaller than all the antennas [9, 11–15, 17, 19–22] and exhibits higher isolation than antenna structures reported in [11–14, 17]. The structures designed in [9, 15, 19–22] offer higher isolation but also occupy a large area. [9] offers low isolation in upper band; [15, 19–22] offer higher isolation, but these structures are electrically two to five times larger in size. The antenna is simple to design, easy to fabricate, and low in cost. It offers stable radiation patterns and adheres to all the diversity parameters and MIMO standards.

5. CONCLUSION

A simple and compact dual-band MIMO antenna with high isolation for GSM 1800 and WLAN applications is designed consisting of two mirror-image monopole radiating elements. Each element consists of a quarter annual ring and an inverted U-shaped strip. Extended ground plane stubs and ground slots are incorporated to achieve isolation $>$ 20 dB over 1.704–1.934 GHz and $>$ 28 dB over 5.66–6.25 GHz frequency range. The antenna is simple to design, easy to fabricate, and low in cost. It offers stable radiation patterns and adheres to all diversity parameters and MIMO standards.

REFERENCES

1. Jensen, M. A. and J. W. Wallace, "A review of antennas and propagation for MIMO wireless communications," *IEEE Transactions on Antennas and Propagation*, Vol. 52, No. 11, 2810–2824, November 2004.
2. Zhao, L. and K. L. Wu, "A dual-band coupled resonator decoupling network for two coupled antennas" *IEEE Transactions on Antennas Propagation*, Vol. 63, No. 7, 2843–2850, 2015.
3. Nadeem, I. and D. Y. Choi, "Study on mutual coupling reduction technique for MIMO antennas," *IEEE Access*, Vol. 7, 563–586, 2019.

4. Chouhan, S., D. K. Panda, M. Gupta, and S. Singhal. "Multiport MIMO antennas with mutual coupling reduction techniques for modern wireless transreceive operations: A review," *International Journal of RF and Microwave Computer-Aided Engineering*, Vol. 28, No. 2, 2017.
5. Moghadasi, M. N., R. Ahmadian, Z. Mansouri, F. B. Zarrabi, and M. Rahimi, "Compact EBG structures for reduction of mutual coupling in patch antenna MIMO arrays," *Progress In Electromagnetics Research C*, Vol. 53, 145–154, 2014.
6. Veeramani, A., A. S. Arezomand, J. Vijayakrishnan, and F. B. Zarrabi, "Compact S-shaped EBG structures for reduction of mutual coupling," *2015 Fifth International Conference on Advanced Computing & Communication Technologies*, 21–25, Haryana, India, 2015.
7. Naderia, M., F. B. Zarrabib, F. S. Jafaric, and S. Ebrahimid, "Fractal EBG structure for shielding and reducing the mutual coupling in microstrip patch antenna array," *International Journal of Electronics and Communications*, Vol. 93, 261–267, 2018.
8. Dharmarajan, A., P. Kumar, and T. J. O. Afullo, "A high gain UWB human face shaped MIMO microstrip printed antenna with high isolation," *Multimedia Tools and Application*, Vol. 81, 34849–34862, 2022.
9. Hussain, R., M. U. Khan, and M. S. Sharawi, "An integrated dual MIMO antenna system with dual-function GND-plane frequency-agile antenna," *IEEE Antennas and Wireless Propagation Letters*, Vol. 17, No. 1, 142–145, January 2018.
10. Chandel, R., A K. Gautam, and K. Rambabu "Tapered fed compact UWB MIMO-diversity antenna with dual band-notched characteristics," *IEEE Transactions on Antennas and Propagation*, Vol. 66, No. 4, 1677–1684, April 2018.
11. Nirmal, P. C., A. Nandgaonkar, S. Nalbalwar, and R. K. Gupta, "A compact dual band mimo antenna with improved isolation for WI-MAX and WLAN applications," *Progress In Electromagnetics Research M*, Vol. 68, 69–77, 2018.
12. Nirdosh, A. Kakkar, M. R. Tripathy, and A. K. Singh. "A novel compact two element MIMO antenna with pie shaped slot structure for dual band applications," *IEEE Progress In Electromagnetics Research Symposium, Singapore*, 336–341, November 19–22, 2017.
13. Tiwari, R.N., P. Singh, S. Pandey, R. Anand, D. K. Singh, and B. K. Kanaujia, "Swastika shaped slot embedded two port dual frequency band MIMO antenna for wireless applications," *Analog Integrated Circuits and Signal Processing*, Vol. 109, 103–113, Springer Nature, 2021.
14. Lin, X. J., Y. Zheng, Y. F. Wang, and Y. X. Lai, "Compact dual band mimo antenna with high isolation," *2019 Photonics & Electromagnetics Research Symposium — Fall (PIERS FALL)*, 804–808, Xiamen, China, December 17–20, 2019.
15. Wang, W., Y. Wu, W. Wang, and Y. Yang, "Isolation enhancement in dual-band monopole antenna for 5G applications," *IEEE Transactions on Circuits and Systems*, Vol. 68, No. 6, 1867—1871, June 2021.
16. Bait-Suwailam, M. M., T. Almoneef, and S. M. Saeed, " Wideband MIMO antenna with compact decoupling structure for 5G wireless communication applications," *Progress In Electromagnetics Research Letters*, Vol. 100, 117–125, 2021.
17. Dou, Y., Z. Chen, J. Bai, Q. Cai, and G. Liu, "Two-port CPW-fed dual-band MIMO antenna for IEEE 802.11 a/b/g applications," *Hindawi International Journal of Antennas and Propagation*, Vol. 2021, Article ID 5572887, 10 June 2021.
18. Achariparambil, A., K. K. Indhu, R. A. Kumar, K. Neema, and A. Chandroth, "Ultra-wideband quad element MIMO antenna on a flexible substrate for 5G and wearable applications," *Progress In Electromagnetics Research C*, Vol. 126, 143–155, 2022.
19. Yahya, L. S., L. S. Yahya, and K. H. Sayidmarie, "A crescent-shaped monopole mimo antennas with improved isolation for dual-band wlan applications," *Progress In Electromagnetics Research C*, Vol. 117, 115–127, 2021
20. Panda, A. K., S. Sahu, and R. K. Mishra, "A compact dual-band 2×1 metamaterial inspired mimo antenna system with high port isolation for LTE and WiMax applications," *International Journal of RF and Microwave Computer-Aided Engineering,* Vol. 27, No. 8, 2017.

21. Biswal, S. P. and S. Das, "Two-element printed PIFA-MIMO antenna system for WiMAX and WLAN applications," *IET Microw. Antennas Propag.*, Vol. 12 No. 14, 2262–2270, 2018.
22. Deng, J. Y., Z. J. Wang, J. Y. Li, and L. X. Guo, "A dual-band MIMO antenna decoupled by a meandering line resonator for WLAN applications," *Microw. Opt. Technol. Lett.*, Vol. 60, No. 3, 759–765, 2018.
23. Naidu, P. V., D. Maheshbabu, A. Saiharanadh, A. Kumar, N. Vummadisetty, L. Sumanji, and K. A. Meerja, "A compact four-port high isolation hook shaped ACS fed MIMO antenna for dual frequency band applications," *Progress In Electromagnetics Research C*, Vol. 113, 69–82, 2021.
24. Dileepan, D., S. Natarajan, and R. Rajkumar, "A high isolation multiband MIMO antenna without decoupling structure for WLAN/WiMAX/5G applications," *Progress In Electromagnetics Research C*, Vol. 112, 207–219, 2021.
25. Naidu, P. V., A. Saiharanadh, D. Maheshbabu, A. Kumar, and N. Vummadisetty, "Design and performance analysis of G-shaped compact ACS fed 4-port MIMO antenna for triple frequency band applications," *Progress In Electromagnetics Research C*, Vol. 112, 55–68, 2021
26. Yang, M., and J. Zhou, "A compact pattern diversity MIMO antenna with enhanced bandwidth and high-isolation characteristics for WLAN/5G/WiFi applications," *Microw Opt. Technol. Lett.*, Vol. 62, No. 6, 2353–2364, 2020.
27. Pradeep, P., J. S. Kottareddygari, and C. S. Paidimarry, "A compact 4×4 peace-shaped wideband MIMO antenna for sub-6 GHz 5G wireless applications," *International Journal of Microwave and Optical Technology*, Vol. 17, No. 5, September 2022.
28. Khade, A., M. Trimukhe, S. Jagtap, and R. K. Gupta, "A circular sector with an inverted L-shaped monopole antenna for tri-band applications," *Progress In Electromagnetics Research C*, Vol. 118, 177–186, 2022.
29. Sharawi, M., "Printed multi-band mimo antenna systems and their performance metrics [Wireless Corner]," *IEEE Antennas and Propagation Magazine*, Vol. 55, No. 5, 218–232, 2013.